Acta Crystallographica Section D
Biological Crystallography
ISSN 0907-4449

Crystallization and preliminary crystallographic studies of the NCoA-1/SRC-1 PAS-B domain bound to the L*XX*LL motif of the STAT6 transactivation domain

Adelia Razeto,[a] Edith Pfitzner[b] and Stefan Becker[a]*

[a]Department for NMR-Based Structural Biology, Max Planck Institute for Biophysical Chemistry, Am Fassberg 11, 37077 Göttingen, Germany, and [b]Georg-Speyer-Haus, Institute for Biomedical Research, Paul-Ehrlich-Strasse 42-44, 60596 Frankfurt, Germany

Correspondence e-mail: sabe@nmr.mpibpc.mpg.de

Received 1 December 2003
Accepted 18 December 2003

Signal transducer and activator of transcription 6 (STAT6) regulates transcriptional activation in response to interleukin-4 (IL-4) by direct interaction with coactivators. Among them, NCoA-1, a member of the p160/steroid receptor coactivator (SRC) family, has been found to bind to STAT6 with the region B of its putative Per–Arnt–Sim (PAS) domain. STAT6 interacts specifically with NCoA-1 *via* an L*XX*LL motif in its transactivation domain. Crystals of the NCoA-1(257–385) domain in complex with the STAT6(794–814) L*XX*LL motif were obtained in two hexagonal space groups. The crystals in space group $P6_1$, with unit-cell parameters $a = 61.7$, $b = 61.7$, $c = 146.5$ Å, $\alpha = \beta = 90$, $\gamma = 120^\circ$, diffract to 2.8 Å at a home source. Crystals belonging to space group $P6_2$, with unit-cell parameters $a = 62.0$, $b = 62.0$, $c = 73.6$ Å, $\alpha = \beta = 90$, $\gamma = 120^\circ$, diffract to 1.8 Å at a synchrotron source.

1. Introduction

STAT proteins (signal transducers and activators of transcription) are mediators of cytokine signalling (Darnell, 1997). Following their specific phosphorylation at a single tyrosine residue by receptor-associated Janus kinases, they dimerize *via* reciprocal binding of the SH2 domain of each monomer to the phosphotyrosine residue of the opposite monomer (Darnell *et al.*, 1994). These dimers are competent to translocate into the nucleus, bind to specific DNA-response elements in the promoter regions of their target genes and regulate transcription. This regulation requires the interactions with components of the transcription machinery. Among them, transcriptional coactivators play a central role as bridging factors between transcriptional activators such as STATs and the basal transcription machinery (Lemon & Tjian, 2000).

The interaction of STATs with coactivators is mediated by their transactivation domains. These domains are relatively proline-rich in all STAT isoforms and are therefore structurally quite flexible (Hoey & Schindler, 1998). So far, no three-dimensional information has been obtained for them: crystal structures of STATs have only been determined with constructs lacking the transactivation domain (Becker *et al.*, 1998; Chen *et al.*, 1998).

STAT6, which mediates the interleukin-4 and interleukin-13 regulated gene expression in immune and anti-inflammatory responses (Smerz-Bertling & Duschl, 1995), has one of the largest transactivation domains found in STATs. It has recently been shown that distinct parts of this transactivation domain interact directly with the coactivators p300/CBP and NCoA-1 (Gingras *et al.*, 1999; Litterst & Pfitzner, 2001, 2002). NCoA-1 belongs to a family of coactivators which are also known as p160/steroid receptor coactivators (SRCs; Leo & Chen, 2000). STAT6 interacts specifically only with NCoA-1, but not with other SRC isomers, *via* an L*XX*LL motif in the C-terminal part of its transactivation domain (Litterst & Pfitzner, 2002). The region of NCoA-1 that is involved in this interaction was identified as region B of a putative Per–Arnt–Sim (PAS) domain.

Here, we report the crystallization and preliminary X-ray studies of the complex between the NCoA-1 PAS-B domain (257–385) and the STAT6 fragment (794–814) containing the L*XX*LL motif.

2. Crystallization

Details of the protein expression and purification will be published elsewhere. The synthetic STAT6 fragment (794–814) was added in twofold excess to the purified NCoA-1 PAS-B domain (257–385). This mixture was loaded onto a Superdex 75 HR 10/30 gel-filtration column (Amersham Biosciences) to remove excess STAT6 fragment. MALDI mass spectrometry confirmed the presence of the STAT6 fragment (794–814) and NCoA-1 PAS-B domain (257–385) in the major elution peak. The equimolar stoichiometry of the complex was verified by N-terminal protein sequencing (Edman, 1970). For crystallization, the complex was concentrated to approximately 19 mg ml^{-1}. A preliminary search for crystallization conditions was performed by the sparse-matrix method

Table 1
Crystallization conditions and crystal forms.

Condition No.	1	2	3	4	
Crystal No.	1	2	3	4	5
Precipitant	25% PEG 4K	25% PEG 4K	20% PEG 4K	20% PEG 3350	
Additive	0.2 *M* NH_4OAc	0.2 *M* NH_4OAc	10% MPD	0.2 *M* LiCl	
Buffer	0.1 *M* MES pH 6.0	0.1 *M* MES pH 6.5	0.1 *M* HEPES pH 7.0	—	
Space group	$P6_2$	$P6_1$	$P6_2$	$P6_2$	$P6_2$
Unit-cell parameters					
a (Å)	62.1	61.7	61.1	62.1	62.0
b (Å)	62.1	61.7	61.1	62.1	62.0
c (Å)	73.6	146.5	73.6	73.4	73.6
Highest resolution (Å)	2.5	2.8	2.1	2.2	1.8
V_M (Å^3 Da^{-1})	2.5	2.4	2.4	2.5	2.5
Solvent content (%)	50	49	48	50	50
Molecules per AU	1	2	1	1	1

Table 2
Data-collection statistics.

Values in parentheses correspond to the outer shell.

Crystal No.	1	2	3	4	5
Space group	$P6_2$	$P6_1$	$P6_2$	$P6_2$	$P6_2$
Resolution (Å)	20–2.5 (2.55–2.50)	2.8 (2.85–2.80)	20–2.1 (2.17–2.10)	19.2–2.21 (2.25–2.21)	20.0–1.8 (1.86–1.80)
Observations	94864	112227	71719	137915	67335
Unique reflections	5565	7693	9163	8138	14934
Completeness† (%)	98.8 (97.0)	99.0 (99.1)	100 (100)	99.7 (98.1)	99.8 (99.9)
Redundancy†	16.8 (16.3)	14.4 (12.6)	7.8 (6.8)	16.8 (16.0)	4.5 (3.1)
$\langle I/\sigma(I)\rangle$†	20.7 (8.7)	20.8 (6.6)	30.8 (5.8)	29.9 (8.7)	39.2 (2.6)
R_{merge}†‡ (%)	9.7 (43.4)	10.0 (44.0)	6.2 (35.5)	8.9 (32.5)	3.2 (39.7)

† Friedel pairs merged. ‡ $R_{merge} = \sum_{hkl}\sum_i |I_i(hkl) - \langle I(hkl)\rangle| / \sum_{hkl}\sum_i I_i(hkl)$.

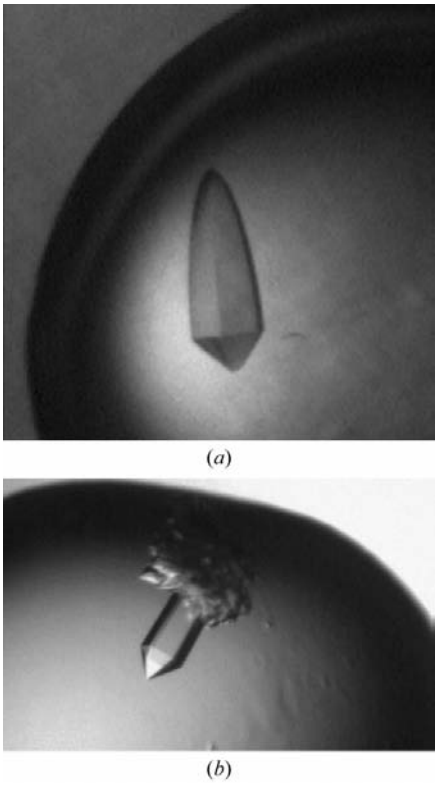

Figure 1
Crystals of NCoA-1(257–385)–STAT6(794–814) grown from 20% PEG 3350 and 0.2 *M* LiCl. (*a*) Crystal No. 4 with dimensions of 0.5 × 0.1 × 0.1 mm. (*b*) Crystal No. 5 with dimensions of 0.7 × 0.4 × 0.4 mm.

(Jancarik & Kim, 1991) using Crystal Screen I (Hampton Research, California, USA). The vapour-diffusion technique was employed in the hanging-drop variant. 1 µl of protein solution was mixed with 1 µl of well solution and equilibrated at 293 K. Irregular multicrystals grew under several conditions.

Fine screening around these conditions was performed by varying the precipitant concentration, buffer type, pH and additives. Crystals of good quality could only be obtained from conditions 1, 2 and 3 (Table 1) by streak-seeding. Crystals appeared 12 d after seeding.

Crystallization trials were also set up using the PEG/Ion screen (Hampton Research). From this screen, crystals suitable for X-ray measurements grew in 1 d under condition No. 4 (Table 1; Fig. 1*a*). Much larger crystals (Crystal No. 5) were subsequently obtained using the same condition with a protein concentration of 22 mg ml^{-1} (Fig. 1*b*).

3. Data collection

To solve the structure of the complex by single-wavelength anomalous diffraction (SAD; Dauter & Dauter, 2001; Dauter *et al.*, 2000), all crystals, except for Nos. 3 and 5 (Table 1), were transferred for 1–3 min into cryoprotectant solutions consisting of the mother liquor containing glycerol at different concentrations (5–25%) and 0.5 *M* NaI. They were then taken up in Hampton cryoloops and directly flash-frozen in liquid nitrogen. Native data sets were collected from crystal 3 and 5. The mother liquor of crystal No. 3 formed an amorphous glass when frozen. Crystal No. 5 was transferred stepwise into mother-liquor solutions with increasing concentrations of glycerol up to 15%. All of the data sets, except for that collected from crystal No. 5, were collected at 100 K using Cu $K\alpha$ radiation from a Siemens rotating-anode generator on a MAR 345 (MAR Research) image-plate detector (Fig. 2). Data from crystal No. 5 were collected at 100 K on the EMBL BW7A synchrotron beamline (DESY, Hamburg) with a MAR CCD image-plate scanner. Data were processed using *DENZO* and *SCALEPACK* (Otwinowski & Minor, 1997). Data statistics are reported in Table 2.

4. Crystallographic analysis

All crystals obtained had a pencil-like shape (a six-sided polyhedron bound to a six-sided pyramid; Fig. 1) and belonged to the hexagonal point group *P*6. However, they were not all isomorphous (Table 1). As estimated by the Matthews coefficient (Matthews, 1968) (Table 1), the asymmetric unit of all crystals contained one molecule, except for crystal No. 2, which belonged to space group $P6_1$. In this case there were two molecules per asymmetric unit and the *c* axis was twice as long as in crystals belonging to space group $P6_2$.

All the crystals soaked in 0.5 *M* NaI showed significant anomalous signal as calculated by *XPREP* (Bruker-AXS, Madison, USA) (Fig. 3). However, for

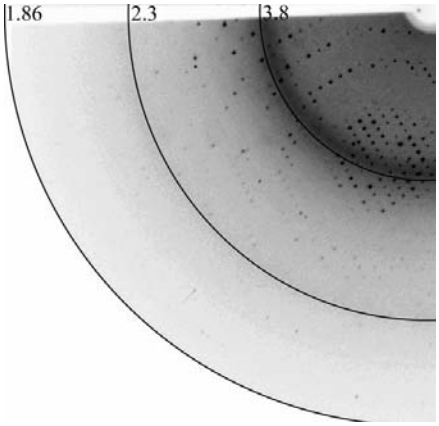

Figure 2
Diffraction image from crystal No. 4.

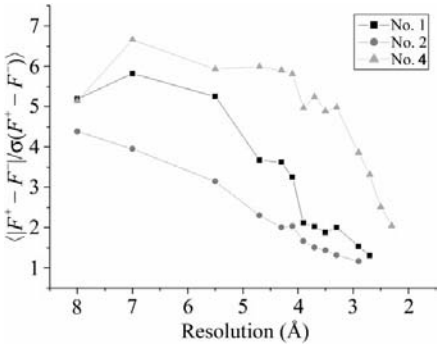

Figure 3
Signal-to-noise ratio $\langle|F^+ - F^-|/\sigma(F^+ - F^-)\rangle$ as a function of resolution.

crystal No. 2 the anomalous signal-to-noise ratio was strong only up to 4.0 Å, which was used as the resolution cutoff to solve the iodide-ion substructure using *SHELXD* (Schneider & Sheldrick, 2002). After 100 dual-space cycles, the correlation coefficient (CC) of the best solution was 51.5 for all data and 24.9 for the weak data not included in the dual-space recycling. However, phase extension and improvement by density modification, performed for both heavy-atom enantiomorphs in *SHELXE* (Sheldrick, 2002), did not result in a clear discrimination between them, even after 100 cycles (contrast/connectivity of 0.648/0.738 and 0.710/0.804).

For crystal No. 1 the resolution cutoff was set to 3.5 Å to search for iodide ions. The CC of the best solution was 45.2 for all data and 22.4 based on the weak data. Only after ten cycles of density modification did the two heavy-atom enantiomorphs diverge significantly from one another, with values of contrast/connectivity of 0.161/0.773 and 0.655/0.897. However, 100 cycles of automatic model building from experimental phases using *ARP*/*wARP* (Perrakis *et al.*, 1999) alternating with *REFMAC* refinement (Murshudov *et al.*, 1997; 500 refinement cycles in total) resulted in tracing only 59 residues out of the total of 153 in ten different chains. The maps were not easily interpretable, most probably owing to the limited resolution and poor data quality.

Crystal No. 4 presented the best anomalous signal-to-noise ratio throughout the entire resolution range (Fig. 3). The iodide substructure was solved using *SHELXD* (Schneider & Sheldrick, 2002) using a cutoff of 3.0 Å, as the signal abruptly decreased above this resolution. The best solution had a CC of 37.6 and 20.2 for all reflections and for the weak reflections, respectively. Ten cycles of phase extension and improvement performed for both heavy-atom enantiomorphs using *SHELXE* (Sheldrick, 2002) were sufficient to clearly distinguish between them (contrast/connectivity of 0.643/0.922 and 0.050/0.718). In this case the maps showed interpretable features. Automatic model building coupled with *REFMAC* refinement (Murshudov *et al.*, 1997; 500 cycles in total) succeeded in tracing most of the structure: 113 residues in three chains out of the total of 153 in two chains (132 amino acids belong to the NCoA-1 fragment and 21 to the STAT6 peptide). Even at the synchrotron source the larger crystal (Fig. 1*b*) obtained under condition No. 4 did not diffract better than 1.8 Å resolution. Data from this crystal might be useful to ultimately obtain a more precise model.

We thank Karin Giller for technical assistance, Dr Hartmut Kratzin for protein sequencing, Kerstin Overkamp for peptide synthesis and Dr Henning Urlaub and Uwe Plessmann for MALDI mass spectrometry. AR and SB were supported by Max-Planck-Gesellschaft and Deutsche Forschungsgemeinschaft (grant Be 2345).

References

Becker, S., Corthals, G. L., Aebersold, R., Groner, B. & Muller, C. W. (1998). *FEBS Lett.* **441**, 141–147.
Chen, X., Vinkemeier, U., Zhao, Y., Jeruzalmi, D., Darnell, J. E. Jr & Kuriyan, J. (1998). *Cell*, **93**, 827–839.
Darnell, J. E. Jr (1997). *Science*, **277**, 1630–1635.
Darnell, J. E. Jr, Kerr, I. M. & Stark, G. R. (1994). *Science*, **264**, 1415–1421.
Dauter, Z. & Dauter, M. (2001). *Structure*, **9**, R21–R26.
Dauter, Z., Dauter, M. & Rajashankar, K. R. (2000). *Acta Cryst.* D**56**, 232–237.
Edman, P. (1970). *Mol. Biol. Biochem. Biophys.* **8**, 211–255.
Gingras, S., Simard, J., Groner, B. & Pfitzner, E. (1999). *Nucleic Acids Res.* **27**, 2722–2729.
Hoey, T. & Schindler, U. (1998). *Curr. Opin. Genet. Dev.* **8**, 582–587.
Jancarik, J. & Kim, S.-H. (1991). *J. Appl. Cryst.* **24**, 409–411.
Lemon, B. & Tjian, R. (2000). *Genes Dev.* **14**, 2551–2569.
Leo, C. & Chen, J. D. (2000). *Gene*, **245**, 1–11.
Litterst, C. M. & Pfitzner, E. (2001). *J. Biol. Chem.* **276**, 45713–45721.
Litterst, C. M. & Pfitzner, E. (2002). *J. Biol. Chem.* **277**, 36052–36060.
Matthews, B. W. (1968). *J. Mol. Biol.* **33**, 491–497.
Murshudov, G. N., Vagin, A. A. & Dodson, E. J. (1997). *Acta Cryst.* D**53**, 240–255.
Otwinowski, Z. & Minor, W. (1997). *Methods Enzymol.* **276**, 307–326.
Perrakis, A., Morris, R. & Lamzin, V. S. (1999). *Nature Struct. Biol.* **6**, 458–463.
Schneider, T. R. & Sheldrick, G. M. (2002). *Acta Cryst.* D**58**, 1772–1779.
Sheldrick, G. M. (2002). *Z. Kristallogr.* **217**, 644–650.
Smerz-Bertling, C. & Duschl, A. (1995). *J. Biol. Chem.* **270**, 966–970.